Journal of Controlled Release 385 (2025) 113995

Contents lists available at ScienceDirect

Journal of Controlled Release

journal homepage: www.elsevier.com/locate/jconrel

Liposomal all-trans retinoic acid boosts anti-tumor immunity of radiotherapy via mitigating cancer stemness and remedying tumor microenvironment

Huilan He [a,b,1], Yun Zheng [a,b,1], Jinlong Ji [b], Chunlian Ye [b], Yu Sun [b], Yuwei Peng [a,b], Ying Zhang [a,b,*], Zhiyuan Zhong [a,b,*]

[a] College of Pharmaceutical Sciences, and State Key Laboratory of Radiation Medicine and Protection, Soochow University, Suzhou, China
[b] Biomedical Polymers Laboratory, College of Chemistry, Chemical Engineering and Materials Science, Soochow University, Suzhou, China

ARTICLE INFO

Keywords:
Radiotherapy
Liposomal nanoparticle
Cancer immunotherapy
Cancer stemness
Immunomodulation

ABSTRACT

Radiotherapy (RT) induces immunogenic cell death but also promotes immunosuppression, cancer stemness and immune evasion, thus compromising anti-tumor immune response and leading to cancer recurrence and metastasis. Here, we developed liposomal all-trans retinoic acid nanoparticles (LATRA) to simultaneously mitigate cancer stemness and remedy suppressive tumor microenvironment, which on one hand decreases tumorigenicity and sensitizes tumors to RT and on the other hand stimulates dendritic cell maturation and reprograms macrophages toward a pro-inflammatory M1 phenotype. In murine colorectal tumor model, RT combined with LATRA essentially reduces tumor burden, prevents recurrence and induces a durable immune response with memory effects. Notably, LATRA effectively eradicates residual tumor cells in post-surgery 4T1 breast tumor model, avoiding tumor relapse and lung metastasis. Liposomal all-trans retinoic acid offers a new and promising strategy to empower RT-induced anti-tumor immunity.

1. Introduction

Radiotherapy (RT) is one of the mainstream clinical cancer therapeutic modalities, which induces DNA damage through high-dose X-rays or other forms of ionizing radiation, ultimately leading to apoptosis or necrosis of tumor cells [1]. In recent years, RT has attracted researchers' attention not only for its direct cytotoxic effects but also for its immunomodulatory capacities such as triggering the immunogenic cell death (ICD) of tumor cells, promoting the release of damage-associated molecular patterns (DAMPs), and modulating immune cells within the tumor microenvironment (TME) [2–4]. Through these processes, RT reprograms the TME and initiates anti-tumor immune responses [5,6]. However, despite these advances, extensive studies have revealed that the anti-tumor immunity generated by RT alone is generally insufficient for complete tumor eradication [7–9].

Cancer stem cells (CSCs) are a subpopulation of tumor cells with self-renewal capacity and limited differentiation potential [10]. These cells are highly resistant to RT-induced cell death, contributing to tumor recurrence and metastasis [11]. Additionally, CSCs facilitate immune escape, diminishing the effectiveness of immunotherapies such as immune checkpoint inhibitors [10,12]. Based on these effects, targeting CSCs or reducing the stemness of cancer cells is a promising strategy to improve the efficacy of cancer radio-immunotherapies. Another major challenge for cancer radio-immunotherapies is the immunosuppressive TME, which can be aggravated by RT through polarizing tumor-associated macrophages (TAMs) toward an M2 phenotype and increasing the tumor infiltration of myeloid-derived suppressor cells (MDSCs), further suppressing the anti-tumor immunity and promoting tumor progression [13]. Therefore, strategies that can mitigate cancer stemness while reversing the immunosuppressive TME hold great promise for orchestrating a robust and sustained radio-immunotherapy.

All-trans retinoic acid (ATRA), a bioactive derivative of vitamin A, has been extensively investigated as a differentiating agent in the treatment of acute promyelocytic leukemia [14]. Emerging evidence indicates that ATRA can regulate key signaling pathways involved in the self-renewal and differentiation of cancer cells, thereby attenuating

* Corresponding authors at: College of Pharmaceutical Sciences, and State Key Laboratory of Radiation Medicine and Protection, Soochow University, Suzhou, China.
E-mail addresses: yzhang628@suda.edu.cn (Y. Zhang), zyzhong@suda.edu.cn (Z. Zhong).
[1] These authors contribute equally.

https://doi.org/10.1016/j.jconrel.2025.113995
Received 6 March 2025; Received in revised form 5 June 2025; Accepted 28 June 2025
Available online 30 June 2025

cancer stemness, reducing tumorigenic potential, and enhancing tumor sensitivity to various therapies [15,16]. However, the clinical application of ATRA is limited by its poor bioavailability and rapid metabolic clearance, which necessitates the development of improved delivery systems [17]. Moreover, the relatively weak immunostimulatory effects of ATRA may restrict its broader application in cancer immunotherapies [18].

In this study, we revealed that RT exacerbates cancer cell stemness across multiple murine cancer cell lines, which may potentially diminish the efficacy of RT-induced anti-tumor immunity. To achieve a potent cancer radio-immunotherapy, we developed liposomal ATRA nanoparticles (LATRA) with two functions: reducing cancer stemness and stimulating immune activation. LATRA effectively attenuated cancer cell stemness, thereby reducing their tumorigenic potential and sensitizing them to therapies. Furthermore, liposomal encapsulation enabled ATRA to promote dendritic cells (DCs) maturation and polarize macrophages toward the pro-inflammatory M1 phenotype (Fig. 1a). Through these effects, LATRA reprogrammed the TME, enhanced anti-tumor T cell activation, and overcame RT-induced immune escape mechanism. In murine tumor models, the combination of LATRA and RT exhibited robust therapeutic efficacy, generating a potent systemic immune response with memory effects. These findings suggest that LATRA represents a promising strategy capable of mitigating cancer stemness and reversing the immunosuppressive TME, two key obstacles confronted by RT, thereby enhancing cancer radio-immunotherapy and advancing personalized treatment strategy.

2. Results

2.1. LATRA effectively attenuates radiation-induced cancer stemness

RT has been reported to induce CSCs-like characteristics, including dedifferentiation, self-renewal and the promotion of oncogenic metabolism through the activation of epithelial-mesenchymal transition (EMT)-inducing pathways [19–21]. In this study, we first investigated whether RT affects the stemness in murine cancer cells. We irradiated cancer cells with a 12 Gy dose, which we previously identified as optimal for enhancing cancer cell immunogenicity and priming anti-tumor immunity [22]. Analysis of irradiated cancer cells revealed a significant upregulation of *Oct4*, a well-established marker of stemness [23], across multiple murine cancer cell lines, including MC38 colorectal cancer cells, 4T1 breast cancer cells, LLC lung cancer cells, and ID8 ovarian cancer cells (Fig. 1b). These results suggest that cancer stemness may serve as a negative feedback mechanism to RT, potentially limiting its therapeutic efficacy.

ATRA could attenuate cancer cell stemness [24]. Here, we developed a liposome-encapsulated formulation, termed LATRA, to overcome the poor solubility of ATRA (Fig. S1 and Table S1). Dynamic light scattering (DLS) and transmission electron microscopy (TEM) images revealed that LATRA had a uniform particle size distribution with a hydrated particle size of approximately 190 nm (Fig. 1c). Additionally, LATRA exhibited excellent storage stability for long-term preservation (Fig. S2). Notably, LATRA exhibited negligible cytotoxic and effective cellular uptake, supporting its potential for therapeutic applications (Figs. 1d and S3). Furthermore, cumulative release studies under different pH conditions revealed a sustained release profile of ATRA from LATRA, with faster release observed at acidic pH (pH 5.5) compared to neutral conditions (pH 7.4), indicating its potential for pH-responsive drug delivery within the tumor microenvironment (Fig. 1e).

Next, we evaluated the efficacy of LATRA in mitigating the cancer cell stemness. As shown in Fig. 1f-g, similar to ATRA, LATRA significantly downregulated the expression of *Oct4* and *Nanog* in both irradiated MC38 and irradiated 4T1 cells, indicating that LATRA effectively suppressed RT-induced stemness. These findings demonstrate that LATRA not only improves aqueous solubility and biocompatibility but also retains the CSC-differentiating effects of ATRA, highlighting its potential as a promising platform for cancer therapy.

2.2. LATRA reduces cancer cell migration and tumorigenicity and enhances radiosensitivity

CSCs have been shown to be essential for the recurrence and metastasis of cancer [25]. Given our findings that LATRA mitigated RT-induced cancer stemness, we next investigated its potential on cancer cell migration and tumorigenicity. The wound healing assay, a common method to evaluate cell migration [26], revealed untreated cancer cells rapidly migrated, reducing the wound area within 24 h (Figs. 2a and S4). At 48 h, cell migration in the RT group was comparable to that of the PBS group, suggesting that the initial inhibitory effect of RT, likely resulting from acute DNA damage, was not sustained over time. In contrast, the addition of LATRA effectively inhibited wound healing in both untreated and irradiated cancer cells (Fig. S5). This inhibitory effects on cancer cell migration may be associated with the ability of LATRA to reduce cancer stemness, a key regulator of metastatic potential. These findings suggest that LATRA holds promise in preventing cancer metastasis.

Next, we examined the impact of LATRA on the self-renewal and tumorigenicity of cancer cells. As shown in Fig. 2b, treatment with LATRA significantly reduced the number of colonies formed by MC38 cells, particularly when combined with RT. Similar results were observed in the tumor sphere formation assay, which reflects the self-renewal and differentiation potential under low-adhesion conditions [24]. LATRA alone decreased tumor sphere size, and the combination of LATRA and RT further disintegrated tumor spheres, with cells exhibiting a single-cell morphology (Figs. 2c-e and S6). These results suggest that LATRA reduces the self-renewal and tumorigenicity of cancer cells.

To explore the radiosensitizing effects of LATRA, we assessed DNA damage by measuring the fluorescence signal of γH2AX, a marker of DNA double-strand breaks. While LATRA alone exhibited negligible effects on DNA damage and RT alone induced considerable γH2AX signal accumulation, their combination produced a markedly enhanced γH2AX signal (Fig. 2f). These findings indicate that LATRA potentiates RT-induced DNA damage, thereby enhancing the tumor cell response to radiation.

2.3. LATRA modulates immune cell populations in vitro

We investigated the immunostimulatory effects of ATRA, blank liposomes (Lipo) and LATRA on bone marrow-derived dendritic cells (BMDCs), which play crucial roles in priming adaptive anti-tumor immunity [27]. Flow cytometry analysis revealed that while ATRA had a negligible effect on DCs activation, LATRA significantly increased the proportion of $CD80^{+}CD86^{+}$ BMDCs (Figs. 3a and S7). Furthermore, enzyme-linked immunosorbent assay (ELISA) analysis of the supernatant collected from BMDCs showed a corresponding increase in IL-6 and decrease in IL-10 secretion following LATRA treatment (Figs. 3b and S8). These results indicated that liposomal encapsulation plays a pivotal role for LATRA in enhancing DCs activation and cytokine production.

TAMs are key regulators of the tumor immune microenvironment. M1 macrophages promote anti-tumor immunity by secreting pro-inflammatory cytokines and activating T cells, whereas M2 macrophages support immune evasion by producing immunosuppressive cytokines [28,29]. Previous studies have demonstrated that certain lipid-based drug delivery systems can effectively reprogram TAMs, enhance nanoparticle uptake by macrophages and reprogram the immunosuppressive TME [30]. As shown in Figs. 3c-d and S9-S11, ATRA alone exhibited weak effects on macrophage polarization under our experimental conditions. In contrast, both Lipo and LATRA significantly increased the proportion of $CD86^{+}CD206^{-}$ M1 macrophages, reduced the proportion of $CD206^{+}$ M2 macrophages, and upregulated the secretion of IL-6 from bone marrow-derived macrophage (BMDMs). These findings indicate a clear shift toward the M1 (pro-inflammatory)

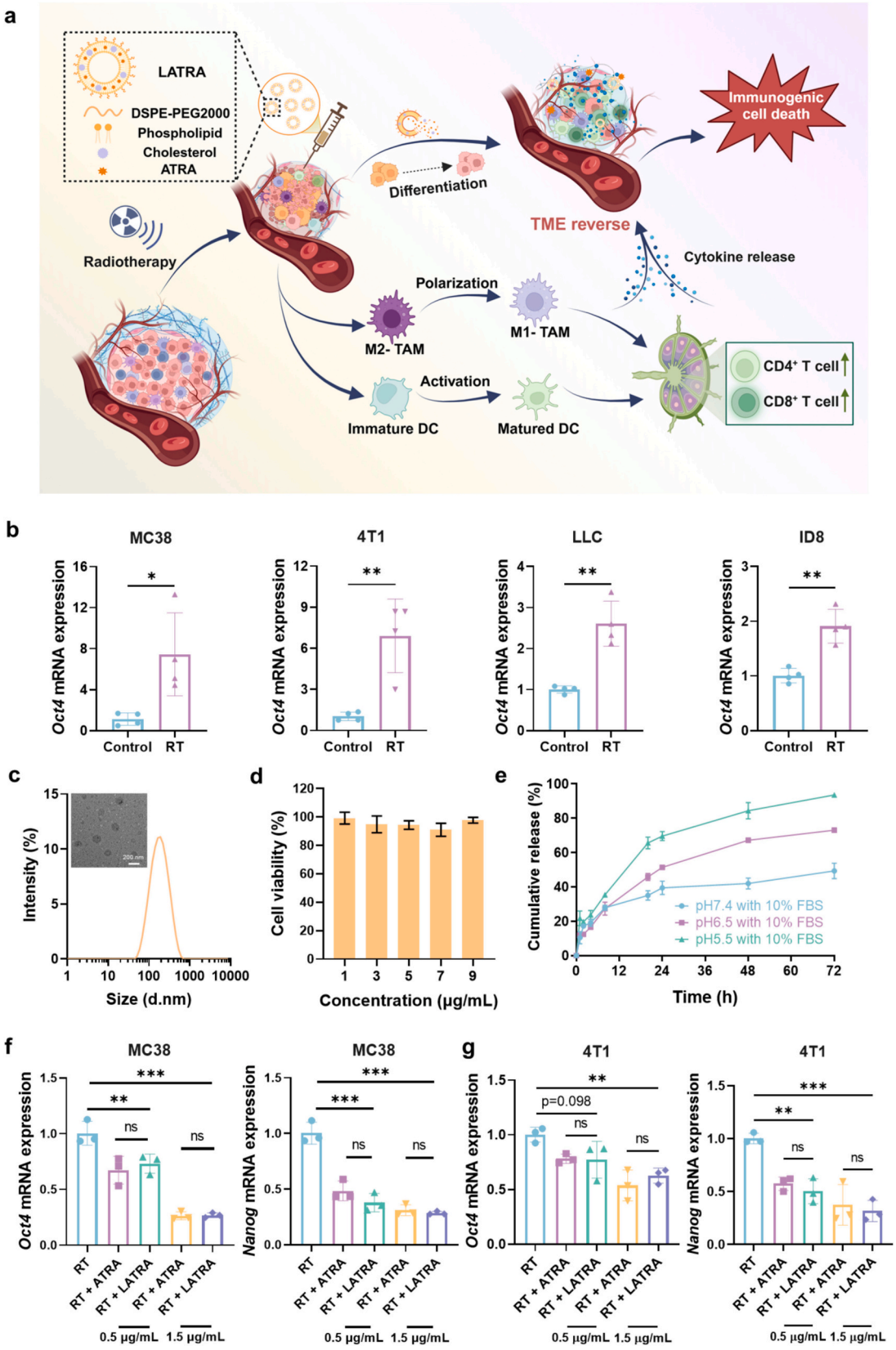

Fig. 1. (a) Composition of LATRA and its mechanism of action in TME modulation. (b) The relative mRNA expression of *Oct4* in MC38 cells, 4T1 cells, LLC cells and ID8 cells after treatment with RT ($n = 4$). (c) The size distribution and representative TEM image of LATRA. (d) The cell viability of MC38 cells treated with different concentrations of LATRA ($n = 5$). (e) Cumulative release profile of ATRA from LATRA in phosphate buffer solutions with different pH values ($n = 3$). (f) The relative mRNA expression of *Oct4* and *Nanog* in irradiated MC38 cells at 48 h, following treatment with ATRA or LATRA (n = 3). (g) The relative mRNA expression of *Oct4* and *Nanog* in irradiated 4T1 cells at 48 h, following treatment with ATRA or LATRA (n = 3). Statistical significance was calculated via unpaired *t*-test in b, and one-way ANOVA test in f-g. $^{*}p < 0.05$, $^{**}p < 0.01$, $^{***}p < 0.001$.

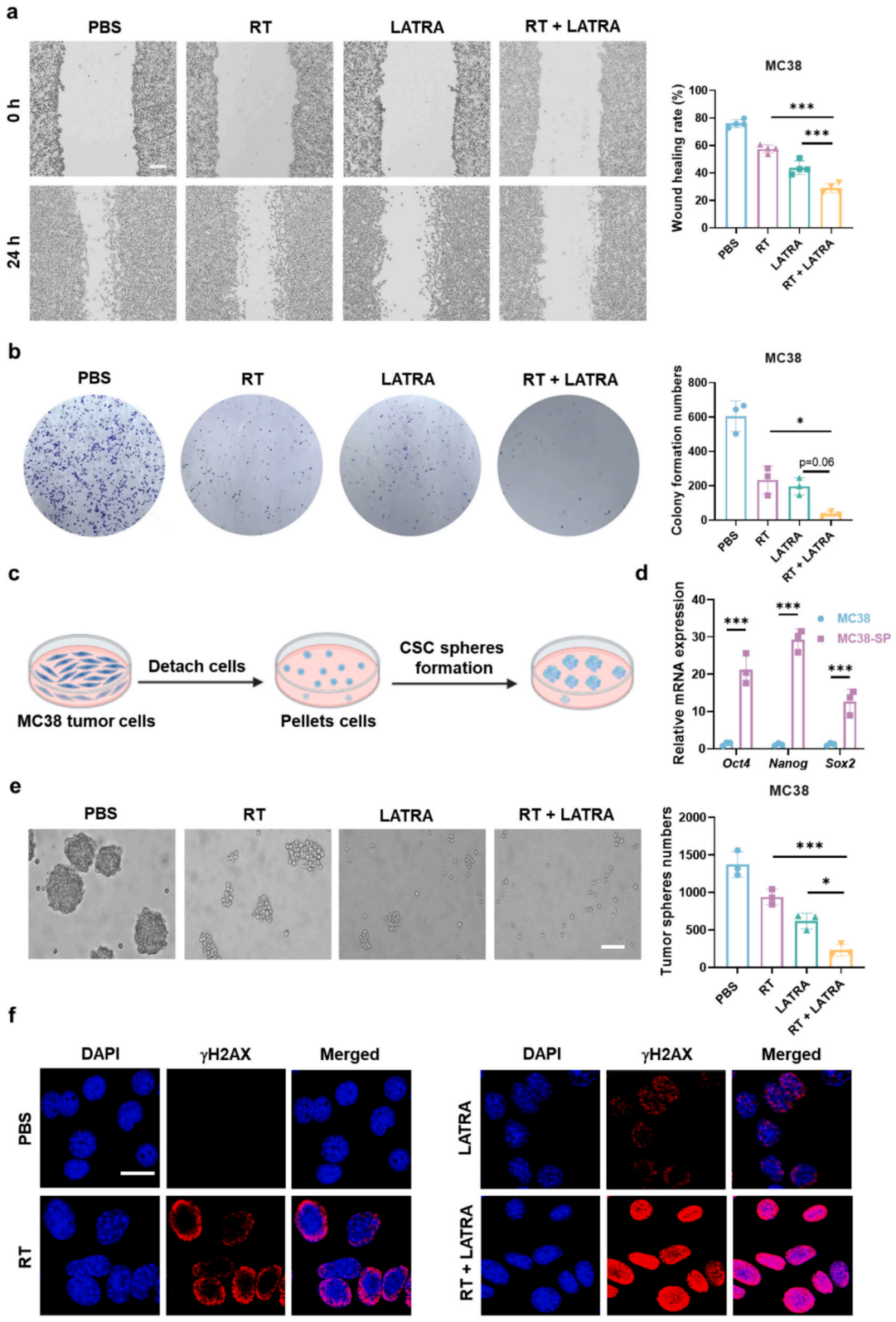

Fig. 2. (a) Representative images from a wound healing assay and relative wound healing rates of MC38 cell cultures treated with RT, LATRA or their combination ($n = 4$). Scale bar = 100 μm. (b) Representative images of clonogenic formation in MC38 cells and the numbers of colonies after treatment with RT, LATRA or their combination ($n = 3$). (c) Schematic illustration of the tumor sphere formation studies. (d) The relative mRNA expression of *Oct4*, *Nanog* and *Sox2* in MC38 spheres (n = 3). (e) Representative images of MC38 cell spheres and the number of spheres after treatment with RT, LATRA or their combination (n = 3). Scale bar = 100 μm. (f) Fluorescence images of the cell nucleus (DAPI) and DNA damage (γH2AX) in MC38 cells after treatment with RT, LATRA or their combination. Scale bar = 20 μm. Statistical significance was calculated via one-way ANOVA test in a-b and e, and unpaired *t*-test in d. $^{*}p < 0.05$, $^{**}p < 0.01$, $^{***}p < 0.001$.

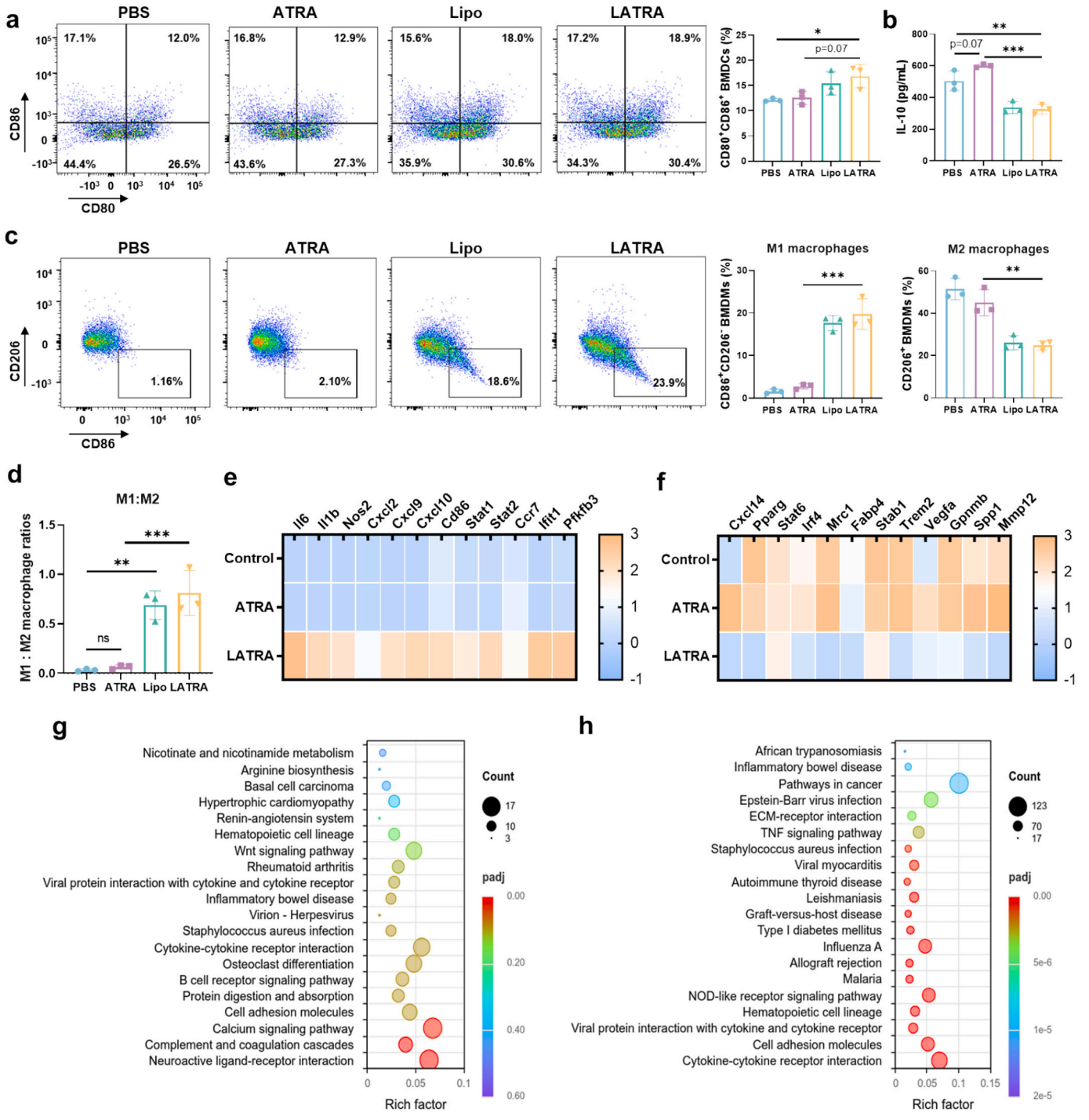

Fig. 3. (a) Representative flow cytometry analysis and quantitative analysis of the activation of BMDCs after treatment with ATRA, Lipo or LATRA ($n = 3$). (b) The concentration of IL-10 in the supernatant of BMDCs after indicated treatment (n = 3). (c) Representative flow cytometry analysis of CD86 and CD206 on BMDMs, and quantitative analysis of M1 ($CD86^+CD206^-$) and M2 ($CD206^+$) phenotypes among BMDMs after treatment with ATRA, Lipo or LATRA (n = 3). (d) Ratios of M1:M2 BMDMs after indicated treatment (n = 3). (e) Heatmaps of the expression of different genes associated with M1 polarization in BMDMs after treatment with ATRA or LATRA. (f) Heatmaps of the expression of different genes associated with M2 polarization in BMDMs after treatment with ATRA or LATRA. (g) KEGG analyses of differentially expressed genes (DEGs) in BMDMs treated with ATRA. (h) KEGG analyses of differentially expressed genes (DEGs) in BMDMs treated with LATRA. Statistical significance was calculated via one-way ANOVA test in a-d. $^*p < 0.05$, $^{**}p < 0.01$, $^{***}p < 0.001$.

phenotype, while LATRA did not show any cytotoxicity on these BMDMs across a range of concentrations. Consequently, the balance of macrophage polarization shifted toward a higher M1/M2 ratio, favoring a pro-inflammatory phenotype. Moreover, as shown in Fig. S12, LATRA significantly increased the expression ratios of *Ifnγ*:*Il4* in T cells, suggesting a shift toward a Th1-dominant immune response. LATRA modulates both macrophages and T cells toward pro-inflammatory phenotypes, further highlighting its potential in enhancing anti-tumor immunity.

To investigate the molecular mechanisms underlying the differential effects of ATRA and LATRA on macrophage polarization, we performed RNA sequencing (RNA-seq) analysis on BMDMs treated with either ATRA or LATRA. Heatmap analysis of differentially expressed genes revealed that LATRA significantly upregulated genes associated with M1

macrophage polarization, while ATRA predominantly upregulated genes linked to M2 macrophage polarization (Fig. 3e-f). Furthermore, Kyoto Encyclopedia of Genes and Genomes (KEGG) pathway enrichment analysis of the top 20 signaling pathways showed that LATRA activated immune-related pathways, whereas ATRA did not significantly enrich immune-associated pathways (Fig. 3g-h). These results suggest that the liposomal formulation of ATRA enabled it to engage distinct immune pathways, thereby promoting M1 macrophage polarization and pro-inflammatory cytokines production, which are key factors in supporting a robust anti-tumor immune response.

2.4. RT + LATRA eradicates MC38 colorectal cancer and prevent cancer relapse

To assess LATRA's tumor microenvironment modulation, intratumoral injection was employed to achieve localized delivery. Biodistribution analysis using Cy5-co-loaded LATRA revealed predominant accumulation in tumor tissue at 4 h post-injection. At 24 h, LATRA still showed sustained retention in the tumor, indicating prolonged and effective therapeutic exposure (Fig. S13). Based on the effects of LATRA in mitigating RT-induced cancer stemness and modulating immune responses, we evaluated the anti-tumor efficacy of LATRA in combination with RT in MC38 colorectal cancer-bearing mice (Fig. 4a). As shown in Figs. 4b-d and S14, treatment with LATRA alone resulted in modest tumor growth inhibition, reflecting its immunomodulatory activity but limited direct cytotoxicity. Tumor growth was also modestly inhibited following RT treatment alone. To further optimize the therapeutic regimen, we investigated the anti-tumor effects treated with different doses of LATRA in combination with RT. As shown in Fig. S15, increasing the dose of LATRA led to progressively enhanced tumor growth suppression when combined with RT, suggesting a dose-dependent therapeutic benefit. Based on these findings, the higher effective dose was selected for subsequent experiments. Notably, the combination of RT and LATRA resulted in a markedly enhanced anti-tumor effect, with 80% of the treated mice achieving complete tumor regression. Importantly, the superior therapeutic outcomes observed in the RT + LATRA group compared to the RT + ATRA group highlight the significance of the immunomodulatory properties of LATRA in enhancing its anti-tumor efficacy. The mice exhibited negligible changes in body weight (Fig. 4e) and hematoxylin and eosin (H&E) staining of major organs showed no significant histopathological abnormalities (Fig. S16), indicating good biocompatibility of both RT + ATRA and RT + LATRA treatments. Histological analysis of tumor tissues via H&E staining revealed that RT + LATRA induced extensive structural damage, characterized by widespread necrosis, loss of tumor cell integrity and a substantial reduction in tumor cell density. Fluorescence imaging of tumor sections further demonstrated that both ATRA and LATRA treatments significantly reduced RT-induced OCT4 expression, which confirmed a reduction in tumor stemness (Fig. 4f).

To assess the durability of the immune response induced by RT + LATRA, we re-challenged mice with MC38 tumor cells on day 60 post-treatment, following complete tumor regression. Remarkably, none of the re-challenged mice developed tumors, indicating the establishment of long-term immune memory (Fig. 4g-h). By analyzing the T cells in blood and spleens, we found that local RT + LATRA treatment significantly increased the percentage of $CD44^{+}CD62L^{+}$ central memory T cells (Tcm) within both $CD3^{+}CD4^{+}$ T cell and $CD3^{+}CD8^{+}$ T cell populations in peripheral blood (Fig. 4i). Furthermore, we observed an increase in the proportion of Tem among $CD3^{+}CD4^{+}$ T cells and $CD3^{+}CD8^{+}$ T cells in the spleens, which indicated the enhanced effector function and improved tumor surveillance (Fig. 4j). Overall, these findings demonstrate that LATRA not only enhances the anti-tumor effects of RT but also induces a durable immunity memory response, providing long-term protection against tumor recurrence.

2.5. LATRA reshapes radiation-induced TME and activates systemic anti-tumor immunity

To investigate the immunomodulatory effects of LATRA in vivo, we intratumorally administrated LATRA into irradiated MC38 colorectal cancer-bearing mice and collected tumor tissues, tumor-draining lymph nodes (TDLNs), spleens and blood on day 11 post-treatment initiation. Flow cytometry analysis of tumor tissues revealed significant changes in the abundance and polarization of macrophages. Specifically, the RT + LATRA group exhibited a marked reduction in the proportion of $CD11b^{+}F4/80^{+}$ macrophages and $CD206^{+}$ M2 macrophages in tumor tissues compared to other treatment groups. Although the proportion of $CD86^{+}CD206^{-}$ M1 macrophages remained largely unchanged, the M1/M2 macrophage ratios were significantly increased, suggesting that LATRA promoted macrophage polarization toward the pro-inflammatory M1 phenotype (Fig. 5a-d). Additionally, IL-6 levels in tumor tissue supernatants were significantly elevated following RT + LATRA treatment (Fig. 5e), indicating an enhanced inflammatory response within the TME, which may contribute to tumor growth inhibition through immune activation. Immunofluorescence analysis further confirmed the effects of LATRA in macrophage modulation. In the RT + LATRA group, fluorescent intensity of iNOS (green), an M1 macrophage marker, was markedly increased, indicating enhanced pro-inflammatory activity. In contrast, the expression of ARG1 (red), an M2 macrophage marker, was significantly reduced, suggesting that LATRA effectively suppressed the infiltration or function of M2 macrophage (Fig. 5f). These results support the ability of LATRA to reshape the TME by promoting macrophage polarization toward an immunostimulatory phenotype.

To evaluate whether local RT + LATRA treatment induces a systemic immune response with memory effects, we analyzed immune cell populations in TDLNs, spleens and peripheral blood. In TDLNs, RT + LATRA treatment significantly increased the proportions of activated $CD8^{+}$ T cells and $CD4^{+}$ T cells (Fig. 5g), indicating the activation of adaptive anti-tumor immune responses. In the spleens, LATRA treatment led to a substantial increase in the percentages of both $CD4^{+}$ and $CD8^{+}$ central memory T cells (Tcm) and effector memory T cells (Tem) (Fig. 5h–i), demonstrating its ability to enhance long-term immune surveillance and anti-tumor immune memory. However, the inclusion of LATRA to the treatment regimen did not change the immune memory profiles on RT treated mice, which may be due to the different temporal dynamics. Additionally, LATRA increased the proportion of $CD4^{+}$ and $CD8^{+}$ effector T cells while reducing myeloid-derived suppressor cells (MDSCs) compared to RT alone (Fig. 5j–k). The reduction of these immunosuppressive cells suggests that LATRA counteracts tumor-induced immunosuppression, which may further strengthen anti-tumor immunity. Peripheral blood analysis revealed no significant changes in activated $CD4^{+}$ T cells; however, a notable increase in activated $CD8^{+}$ T cells was observed (Fig. 5l). This suggested that LATRA enhanced systemic cytotoxic T cell responses.

In summary, LATRA significantly modulates immune responses within the TME by promoting macrophage polarization toward an M1 phenotype, enhancing T cell activation with memory effects, and reducing immunosuppressive cell populations. These findings highlight the potential of LATRA as a potent immunomodulating agent in cancer therapy, capable of boosting both local and systemic anti-tumor immunity.

2.6. LATRA combined with RT prevents post-surgical tumor recurrence and metastasis

Surgical resection remains the primary therapeutic approach in oncology. However, despite advances in surgical techniques, post-operative recurrence rates remain high, primarily due to residual tumor cells at surgical margins and the potential for metastasis [31,32]. RT is commonly employed as an adjunctive therapy to eradicate the residual tumor cells that may persist after surgery [33]. To evaluate the effects of

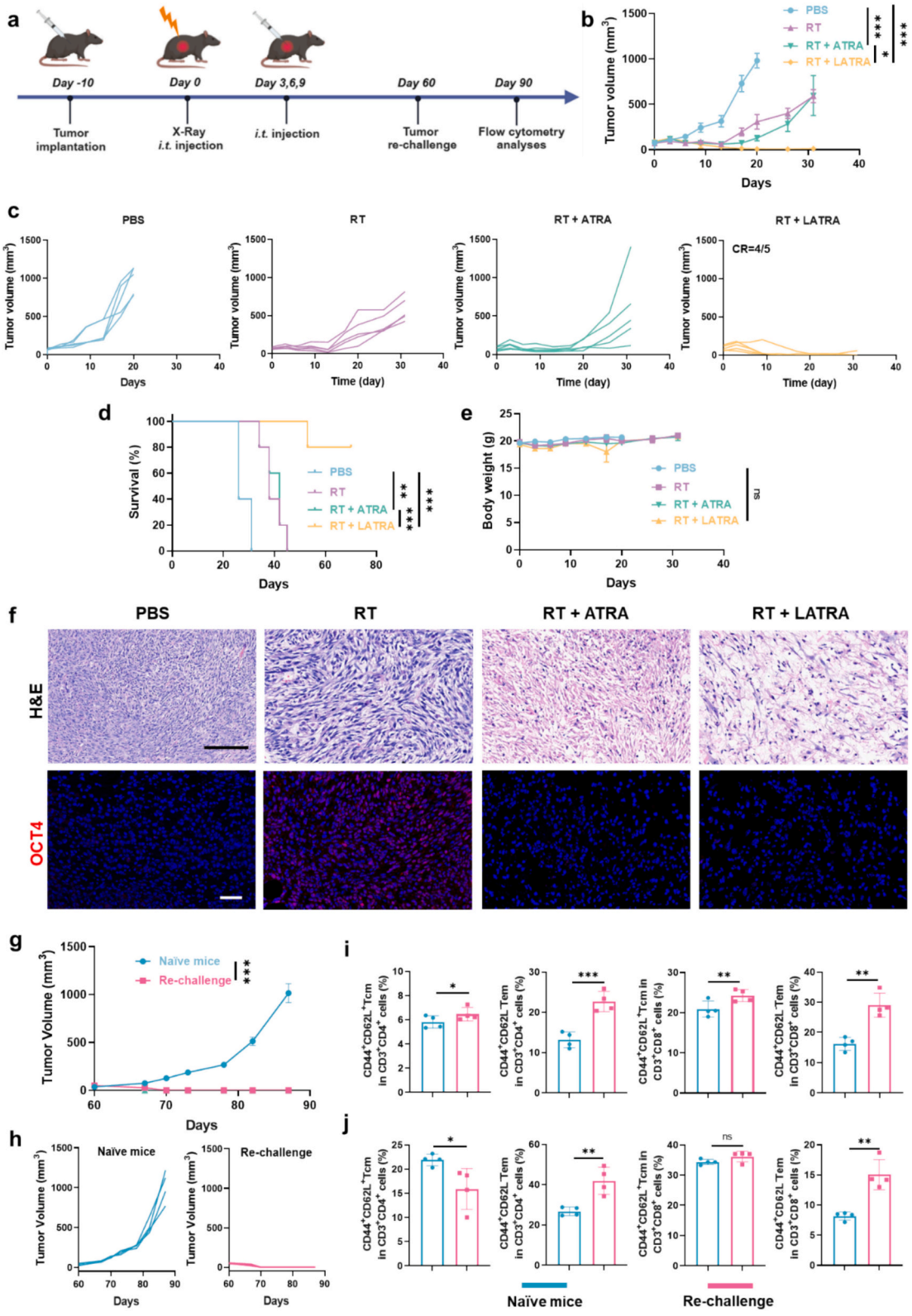

Fig. 4. (a) Scheme for the anti-cancer studies on MC38 colorectal cancer-bearing mice. (b) Average tumor growth curves after indicated treatment ($n = 5$). (c) Individual tumor growth curves in (b). (d) Survival rate and (e) average body weight of mice after indicated treatment (n = 5). (f) H&E staining images (scale bar = 200 μm) and immunofluorescent images (scale bar = 50 μm; blue: DAPI; red: OCT4) of the tumors after indicated treatment. (g) Average tumor growth curves of re-challenged MC38 tumors ($n = 4$). (h) Individual tumor growth curves in (g). (i) The percentages of $CD44^+CD62L^+$ Tcm and $CD44^+CD62L^-$ Tem among $CD3^+CD4^+$ T cells and $CD3^+CD8^+$ T cells in blood (n = 4). (j) The percentages of $CD44^+CD62L^+$ Tcm and $CD44^+CD62L^-$ Tem among $CD3^+CD4^+$ T cells and $CD3^+CD8^+$ T cells in spleen (n = 4). i.t.: Intratumoral. CR: Complete response. Statistical significance was calculated via one-way ANOVA test in b, e, g and i-j, and the log-rank test in d. $^*p < 0.05$, $^{**}p < 0.01$, $^{***}p < 0.001$. (For interpretation of the references to colour in this figure legend, the reader is referred to the web version of this article.)

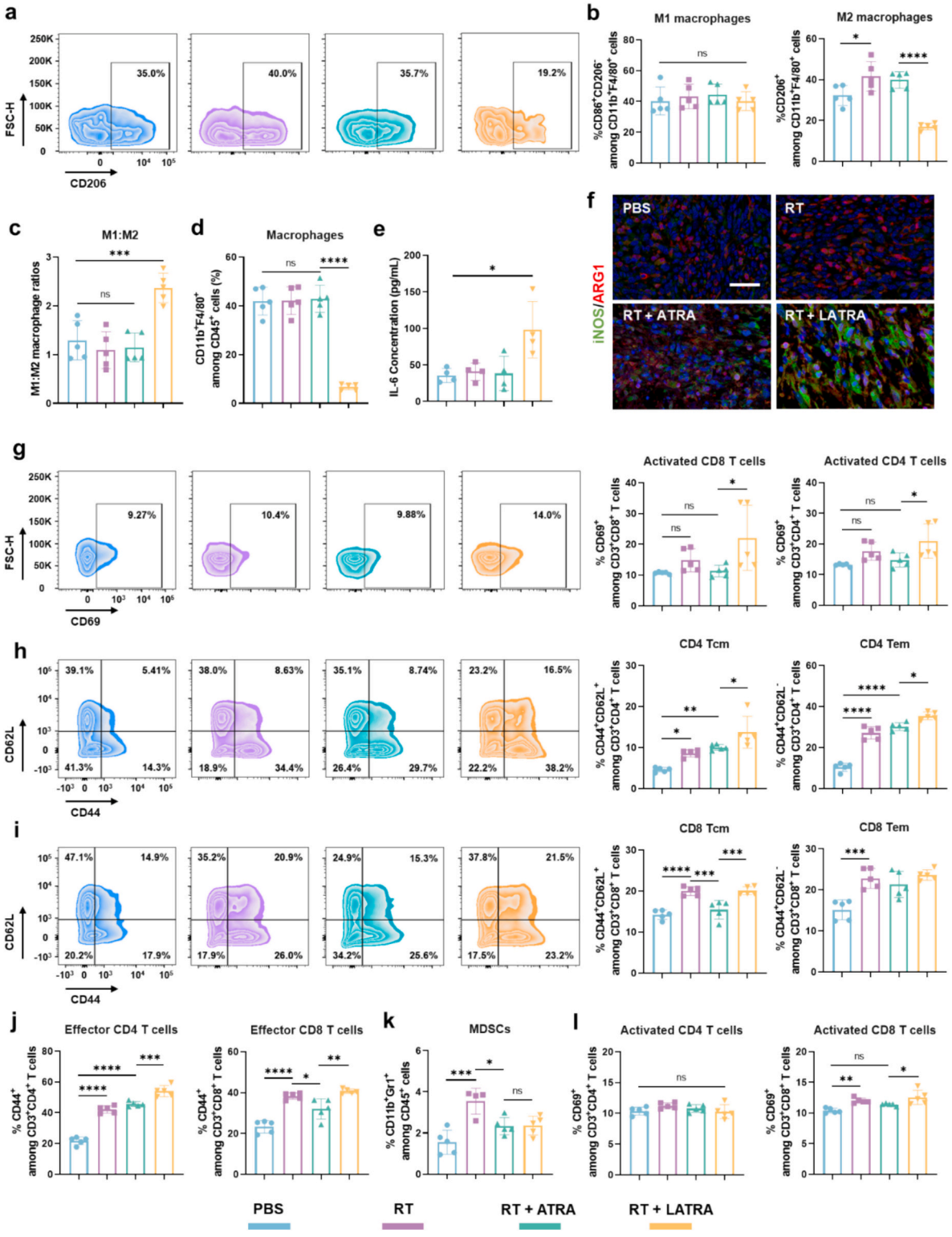

Fig. 5. (a) Representative flow cytometry analysis of $CD206^+$ cells (M2 TAMs) among $CD11b^+F4/80^+$ macrophages in tumor tissues. (b) Percentages of $CD86^+CD206^-$ cells (M1 TAMs) and $CD206^+$ cells (M2 TAMs) among $CD11b^+F4/80^+$ cells in tumor tissues ($n = 5$). (c) Ratios of M1/M2 macrophages in tumor tissues (n = 5). (d) Percentages of $CD11b^+F4/80^+$ macrophages among $CD45^+$ cells in tumor tissues (n = 5). (e) Concentrations of IL-6 in the supernatant of tumor tissues ($n = 4$). (f) Representative immunofluorescence images indicated iNOS and ARG1 in tumor tissues. (g) Representative flow cytometry analysis and percentages of $CD69^+$ cells among $CD3^+CD8^+$ T cells and $CD3^+CD4^+$ T cells in TDLNs (n = 5). Representative flow cytometry analyses and percentages of $CD44^+CD62L^+$ Tcm and $CD44^+CD62L^-$ Tem among (h) $CD3^+CD4^+$ T cells and (i) $CD3^+CD8^+$ T cells in spleens (n = 5). (j) Percentages of $CD44^+$ cells among $CD3^+CD4^+$ T cells and $CD3^+CD8^+$ T cells in spleens (n = 5). (k) Percentages of $CD11b^+$ $Gr\text{-}1^+$ cells among $CD45^+$ cells in spleens (n = 5). (l) Percentages of $CD69^+$ cells among $CD3^+CD4^+$ T cells and $CD3^+CD8^+$ T cells in blood (n = 5). Statistical significance was calculated via one-way ANOVA test in b-e and g-l. $^*p < 0.05$, $^{**}p < 0.01$, $^{***}p < 0.001$.

LATRA in preventing tumor recurrence and metastasis after surgery, we established a post-surgical 4T1-Luc breast cancer mouse model (Fig. 6a). LATRA was incorporated into a clinically used gel (Gel/LATRA) for localized administration at the resection site for sustained release. As shown in Fig. 6b-f, RT alone or in combination with a blank gel modestly delayed tumor progression but failed to prevent recurrence. In contrast, the RT + Gel/LATRA group exhibited almost complete suppression of tumor growth, as evidenced by the absence of luciferase signal and the lack of detectable tumor recurrence.

To further assess the efficacy of RT + Gel/LATRA in preventing tumor metastasis, lung tissues were analyzed on day 30 post-treatment. H&E staining revealed tumor metastasis in the control and RT groups, with the presence of tumor nodules and pathological tissue alterations. In contrast, the RT + Gel/LATRA group showed no detectable metastasis or abnormal histopathological changes in the lungs, indicating that the combination treatment effectively suppressed tumor spread to distant sites (Fig. 6g). These findings highlight the potential of LATRA as an effective adjunct to RT, offering a promising strategy to prevent both post-surgical recurrence and metastasis.

3. Discussion

Despite significant advances in RT for cancer treatment, challenges remain, particularly in preventing tumor recurrence and metastasis post-treatment. Although RT is effective in eliminating the bulk of tumor cells, it often fails to eradicate CSCs, which exhibit inherent resistance to RT-induced anti-tumor immune response. The self-renewal capacity and resistance of CSCs contribute to tumor relapse and metastasis, making them critical targets for therapeutic intervention. Additionally, the TME plays a pivotal role in modulating therapeutic response. Immunosuppressive cells, such as M2 TAMs, further dampen RT-induced anti-tumor immunity. Therefore, strategies that simultaneously target CSCs and reverse tumor immunosuppression are promising approaches for enhancing the efficacy of radio-immunotherapies.

ATRA, a metabolite of vitamin A, regulates key signaling pathways involved in the self-renewal and differentiation of CSCs. In recent years, ATRA has gained attention for its potential to target CSCs and improve oncotherapy outcome [14,34]. For instance, Mo et al. developed nanoparticles co-loaded with ATRA and camptothecin (CPT) to enhance CPT release, reduce stemness-related drug resistance and improve chemotherapy efficacy, leading to suppressed tumor growth and reduced recurrence in breast tumor models [16]. Similarly, Chen et al. designed ultrasound-responsive nanodroplets co-loaded with ATRA and paclitaxel (PTX). This strategy utilized ATRA to reduce cancer stemness and chemoresistance, while ultrasound-induced reactive oxygen species (ROS) generation and aldehyde dehydrogenase (ALDH) downregulation synergistically diminished CSC populations [35]. Additionally, Xiao et al. synthesized a polymer-grafted ATRA nanoparticle (PRA@Oxa-c16). When combined with an anti-PD-L1 antibody, it effectively induced anti-tumor T cell responses, eliminating tumors and preventing their metastasis and recurrence [36]. However, despite these advancements, the application of ATRA to specifically enhance RT-induced immunotherapy by targeting CSCs and modulating the TME remains under explored. The primary focus of those aforementioned studies was predominantly on tumor growth suppression or CSCs inhibition, without directly addressing the distinct challenges associated with RT.

Although RT is a cornerstone of cancer treatment, it paradoxically induces CSCs enrichment and creates an immunosuppressive tumor microenvironment, both of which contribute to therapeutic resistance and tumor recurrence. In this study, we propose a therapeutic strategy using liposomal ATRA (LATRA) designed to mitigate cancer stemness while reversing the immunosuppressive TME, two major barriers to effective radio-immunotherapy. Through these mechanisms, LATRA holds significant potential to induce robust tumor regression and improve patient outcomes, offering a readily translational strategy in clinical cancer treatment.

Our in vitro studies demonstrated that RT significantly enhanced cancer stemness across multiple murine cancer cell lines, an effect effectively mitigated by LATRA. This suggests that targeting CSCs is critical for achieving robust radio-immunotherapy and that LATRA may serve as an efficient agent for reducing cancer stemness (Fig. 1). Further studies confirmed that LATRA-mediated cancer stemness mitigation enhanced tumor cell sensitivity to therapy while suppressing their proliferation and migration (Fig. 2). Moreover, immune cell analyses revealed that the liposomal encapsulation enabled LATRA with potent immunostimulatory effects, including DCs activation, M1 polarization of macrophages, and Th1 polarization of T cells. These immunostimulatory effects were notably absent for free ATRA under the same conditions (Figs. 3 and S3). These findings highlight the necessity of LATRA in augmenting the efficacy of radio-immunotherapy.

In vivo, the combination of LATRA and RT significantly reduced tumor burden and prolonged survival in the MC38 colorectal cancer model compared to RT alone. Notably, this combination not only suppressed tumor recurrence but also induced systemic immune memory, effectively preventing tumor relapse (Fig. 4). Immune profiling further demonstrated that LATRA enhanced the infiltration of immune cells into the TME while reducing the proportion of immunosuppressive cells, such as M2 macrophages. Further analyses revealed that this combinational treatment elicited a systemic anti-tumor immune response with long-term memory effects (Fig. 5). Additionally, LATRA loaded in a clinically used hydrogel combined with RT effectively inhibited tumor recurrence and metastasis in the 4T1 post-surgical breast cancer model (Fig. 6). Overall, these results highlight the critical role of LATRA in modulating the immune microenvironment and enhancing RT efficacy, establishing a promising therapeutic approach for improving cancer radiotherapy outcomes.

In future studies, it would be necessary to investigate the effect of LATRA on enhancing RT efficacy at different radiation doses and evaluate its therapeutic efficacy in orthotopic murine tumor models or patient-derived xenograft (PDX) tumor models. It will be also important to explore the optimal dosing and timing of LATRA administration, as these factors may significantly influence treatment outcomes. Additionally, although LATRA exhibits strong immunostimulatory effects, concerns about immune tolerance or exhaustion in certain tumor microenvironments remain. Addressing these issues will be essential for advancing the clinical potential of LATRA-based radio-immunotherapy. Despite these challenges, our findings provide valuable insights into LATRA as a promising adjuvant to enhance the therapeutic outcome of RT and overcome tumor recurrence and metastasis, highlighting its potential for clinical translation in cancer therapy.

4. Conclusion

In this study, we proposed LATRA as an innovative therapeutic strategy to enhance the efficacy of RT. LATRA effectively mitigated RT-induced cancer stemness, thereby addressing key challenges such as cancer recurrence and metastasis. Additionally, LATRA reprogramed the immune microenvironment by promoting DCs activation, macrophage polarization toward the pro-inflammatory M1 phenotype and enhancing T cell responses. This dual action of LATRA reduced RT-induced immune evasion and immunosuppression, thus improving therapeutic outcomes. By targeting both cancer stemness and tumor immunosuppression, LATRA offers a new approach to overcome the limitations of RT, particularly in tumors resistant to treatment, highlighting its potential in clinical translation.

5. Materials and methods

5.1. Materials

All-trans retinoic acid (ATRA) was obtained from TCI. Cholesterol (>95.0%) and phospholipid (from soybean, >95%) were purchased

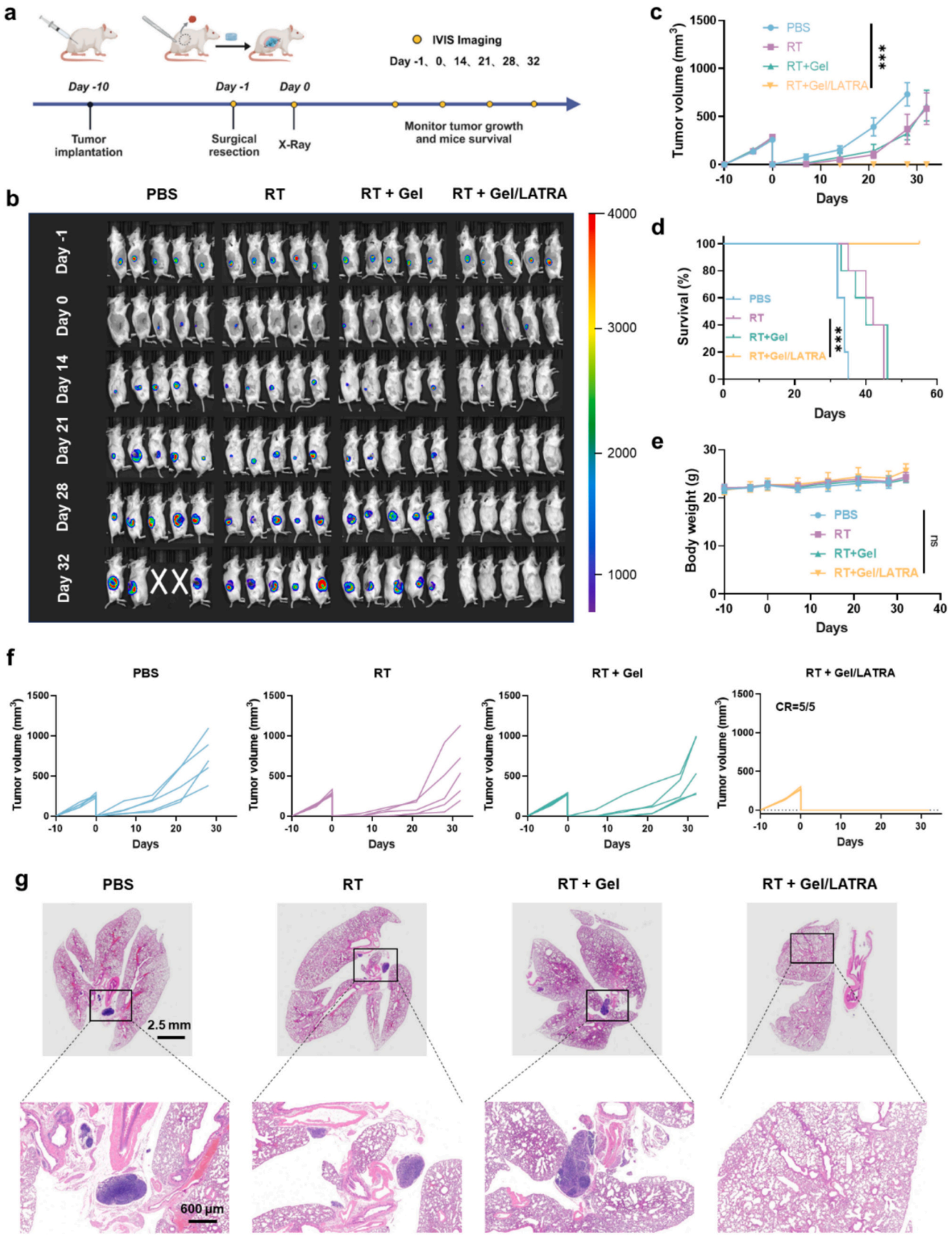

Fig. 6. (a) Scheme for the studies. (b) Bioluminescence images of 4T1-Luc tumor-bearing mice by IVIS. (c) Average tumor growth curves after indicated treatment. (d) Survival rate of mice on days −1, 0, 14, 21, 28 and 32. (c) Average tumor growth curves after indicated treatment ($n = 5$). (d) Survival rate and (e) average body weight of mice after indicated treatment (n = 5). (f) Individual tumor growth curves in (c). (g) H&E staining images of lungs. Statistical significance was calculated via one-way ANOVA test in b-e and g-l. $^{*}p < 0.05$, $^{**}p < 0.01$, $^{***}p < 0.001$. Statistical significance was calculated via the log-rank test in c and e, and log-rank test in d. $^{*}p < 0.05$, $^{**}p < 0.01$, $^{***}p < 0.001$.

from Macklin. DSPE-PEG2000 was purchased from Ponsure. Porcine fibrin sealant was purchased from Guangzhou Bioseal Biotech. D-Luciferin potassium salt was purchased from Aladdin. Recombinant mouse epidermal growth factor (EGF), recombinant mouse basic fibroblast growth factor (bFGF) and B27 supplement were purchased from Yeasen. Methylthiazolyldiphenyl-tetrazolium bromide (MTT) and crystal violet staining solution were purchased from Beyotime Biotechnology. Mouse ELISA kits (IL-6 and IL-10) were purchased from Thermo Fisher Scientific. RNA-easy, HiScript III RT SuperMix for qPCR (+gDNA wiper) and Taq Pro Universal SYBR qPCR Master Mix were obtained from Vazyme. The primer sequences used for RT-qPCR and the antibodies employed for flow cytometry are provided in Tables S2 and S3 of the Supplementary Information.

5.2. Cell lines and tumor models

The MC38, 4T1, LLC,ID8 and 4T1-Luc cell lines were sourced from the National Collection of Authenticated Cell Cultures and cultured in RPMI 1640 medium (Gibco) supplemented with 10% fetal bovine serum (FBS) and 1% penicillin/streptomycin. All cell cultures were incubated at 37 °C in a humidified incubator with 5% CO_2.

Bone marrow-derived dendritic cells (BMDCs) were generated by isolating bone marrow from C57BL/6 mice and culturing the bone marrow cells in RPMI 1640 medium supplemented with 10% FBS, 1% penicillin/streptomycin, 0.1% 2-mercaptoethanol and 20 ng/mL recombinant mouse granulocyte-macrophages colony-stimulating factor (rmGM-CSF) for 7 days. Bone marrow-derived macrophages (BMDMs) were generated using a similar protocol but with 20 ng/mL recombinant mouse macrophages colony-stimulating factor (rmM-CSF). Spleen cells were isolated from C57BL/6 mice, and red blood cells were lysed using ACK lysis buffer. The splenocytes were then re-suspended and cultured in RPMI-1640 medium supplemented with 10% FBS and 1% penicillin for further use. All cell cultures were maintained at 37 °C in a humidified incubator with 5% CO_2.

Female C57BL/6 mice (6–8 weeks) were purchased from the Shanghai Laboratory Animal Center (Shanghai, China). Female Balb/C mice (6–8 weeks) were purchased from the Jiangsu Laboratory Animal Center (Shanghai, China). All animal experiments were approved by the Animal Care and Use Committee of Soochow University, and all protocols conformed to the Guide for the Care and Use of Laboratory Animals. To establish the MC38 colorectal cancer model, female C57BL/6 mice were subcutaneously inoculated with 1×10^6 MC38 colorectal cancer cells on the right flank. To establish the post-surgical 4T1-Luc breast cancer mouse model, female Balb/C mice were subcutaneously inoculated with 3×10^5 4T1-Luc breast cancer cells on the right flank. When the tumor volume reached 200–300 mm^3, tumor resection was performed, followed by subsequent treatments.

5.3. Preparation of LATRA

LATRA was prepared using the thin-film dispersion method. The molar ratio of lecithin, cholesterol and DSPE-PEG2000 was approximately 9:3:1, which was optimized to ensure stable encapsulation. Correspondingly, a mixture of 3 mg ATRA, 27 mg lecithin, 5 mg cholesterol and 13 mg DSPE-PEG-2000 was dissolved in chloroform to obtain the ATRA lipid stock solution. The solution was transferred to a round-bottom flask and chloroform was removed using a rotary evaporator, forming a thin lipid film. The dried lipid film was subsequently hydrated with deionized water to generate a liposome suspension. The suspension was then sonicated using a probe sonicator. Following that, the liposome suspension was extruded through a 200 nm filter using a liposome extruder. Finally, the liposome solution was dialyzed against deionized water to remove unencapsulated free drug. For the blank control, liposomes were prepared using the same procedure but without ATRA. To test the drug loading efficiency, a nine-fold volume of DMSO was added to lyse the liposomes, and then the absorbance was measured at 350 nm. The concentration of ATRA was calculated based on a standard calibration curve prepared in DMSO.

5.4. Cytotoxicity assay

The cytotoxic effect of LATRA was evaluated using the MTT assay. Briefly, MC38 and BMDMs cells were seeded in 96-well plates at a density of 3×10^3 cells per well and incubated overnight. Cells were treated with various concentrations of LATRA for 24 h. Then, 10 μL of MTT solution (5 mg/mL) was added to each well, and plates were incubated for an additional 4 h at 37 °C. Following incubation, the medium was removed, and 100 μL of dimethyl sulfoxide (DMSO) was added to to dissolve the formazan crystals. Absorbance at 450 nm was measured using a microplate reader to determine cell viability, with results expressed as a percentage relative to the control group.

5.5. RNA isolation and quantitative real-time PCR

To evaluate the regulatory effect of radiation on tumor cell stemness, MC38, 4T1, ID8 and LLC cells were seeded at 2×10^5 cells per well in 6-well plates and incubated overnight. Cells were irradiated with 12 Gy X-rays, followed by medium replacement and incubation for 48 h at 37 °C with 5% CO_2. RNA was isolated using RNA-easy and cDNA was synthesized using reverse transcribed using HiScript lll RT SuperMix (+gDNA wiper). Quantitative real-time PCR was performed using Taq Pro universal SYBR qPCR Master Mix on a Bio-Rad CFX Connect system. Gene expression was normalized to *Hprt* using the $2^{-\Delta\Delta Cq}$ method.

For investigating the effect of LATRA on tumor cell stemness, MC38 and 4T1 cells were pre-irradiated as described above, followed by treatment with various concentrations of ATRA (0.5 or 1.5 μg/mL) or the corresponding LATRA formulations (equivalent ATRA doses) for 48 h. Gene expression was analyzed as above.

For T cell activation analysis, single-cell suspensions of spleen cells was seeded at 2×10^6 cells per well in 12-well plates, incubated overnight, and treated with LATRA (ATRA: 1.5 μg/mL) for 24 h. Gene expression was analyzed as above.

5.6. Cellular uptake of LATRA

To prepare Cy5-co-loaded LATRA, Cy5-NHS dissolved in DMSO was added to ATRA lipid stock solution at a mass ratio of 1:25 (Cy5-NHS: LATRA, wt/wt). After the hydration of thin lipid film as mentioned above and the dialysis against deionized water using a dialysis tubing (MWCO: 3.5 kDa), Cy5-co-loaded LATRA was obtained. MC38 cells were seeded into 12-well plates at a density of 2×10^5 cells per well and incubated overnight. Cy5-co-loaded LATRA was then added to the culture medium. After 12 h of incubation at 37 °C, cells were washed with PBS and stained with DAPI for nuclear visualization. Fluorescence imaging was conducted with CLSM to evaluate cellular uptake.

5.7. Wound healing assay

MC38 and 4T1 cells were seeded at 2×10^5 cells per well in 12-well plates and incubated overnight. A uniform scratch was created in the center of each well using a pipette tip. Cells were irradiated with 12 Gy X-rays, followed by media replacement and LATRA treatment (8 μg of ATRA). Cells were then incubated for 24 or 48 h at 37 °C with 5% CO_2. The wound healing was observed under an optical microscope, and images were analyzed using ImageJ software to quantify the changes in scratch area.

5.8. Colony formation assay

MC38 cells were seeded at 600 cells per well in 6-well plates. After incubation for 3–5 days, small cell colonies formed, and were irradiated with 12 Gy X-rays. Following irradiation, LATRA (8 μg of ATRA) was

added, and cells were incubated for an additional 48 h. The cell culture was maintained for 14 days, with media changes every 3 days.Colonies were fixed and stained with crystal violet for 10–20 min, followed by washing and drying. Images were captured, and colonies with diameters greater than 50 μm were quantified using ImageJ software.

5.9. γH2AX staining

MC38 cells were seeded at 3×10^5 cells per well in 6-well plates and incubated overnight. Cells were irradiated with 12 Gy X-rays, followed by media replacement and LATRA treatment (8 μg of ATRA) for 24 h. Cells were then washed, fixed, and blocked to minimize nonspecific binding. Cells were incubated with a primary γH2AX antibody (1:1000) at room temperature for 1 h, then washed and incubated with a fluorescently labeled secondary antibody for 1 h. Followed by washing with PBS for three times, cells were stained with DAPI for 5 min. Finally, cells were mounted with an anti-fade reagent and analyzed under a confocal microscope to assess γH2AX fluorescence signals.

5.10. Tumor sphere formation assay

MC38 and 4T1 cells were harvested at log-phase growth and seeded at 1×10^4 cells per well in 12-well plates with ultra-low attachment surface. Cells were cultured in DMEM/F12 medium supplemented with 20 ng/mL EGF, 20 ng/mL bFGF and 1:50 B27 supplement. Tumor spheres spontaneously formed within 24–48 h, and reached approximately 100 μm in size by day 7. Cells were then irradiated with 12 Gy X-rays and treated with LATRA (ATRA: 1.5 μg/mL) for 24 h. Morphological changes in tumor spheres were observed under a microscope, and the number of spheres larger than 50 μm in diameter was quantified using ImageJ software.

5.11. Maturation of BMDCs

BMDCs were seeded at 1×10^6 cells per well in 12-well plates and incubated overnight. The cells were treated with ATRA, Lipo, or LATRA (8 μg of ATRA). After 24 h, the cells were harvested and incubated with anti-CD16/32 for 10 min. Subsequently, they were stained with anti-CD11c-FITC, anti-CD80-APC and anti-CD86-PE antibodies for flow cytometry analysis.

5.12. Polarization of BMDMs

BMDMs were seeded at 1×10^6 cells per well in 12-well plates and incubated overnight. The cells were treated with LPS (20 ng/mL), ATRA, Lipo, or LATRA (8 μg of ATRA). After 24 h, the cells were harvested and incubated with anti-CD16/32 for 10 min. Subsequently, they were stained with anti-CD11b-FITC, anti-F4/80-PE, anti-CD86-PE/Cy7 and anti-CD206-APC antibodies for flow cytometry analysis.

5.13. RNA-sequencing analyses

BMDMs were seeded at 3×10^6 cells per well in 12-well plates and incubated overnight. The cells were treated with ATRA or LATRA (8 μg of ATRA). After 24 h, total RNA was extracted, converted into a cDNA library, and sequenced by Beijing Novogene Source Technology Co., Ltd. Differential gene expression and enrichment analyses were conducted using the Novogene Cloud platform.

5.14. In vivo biodistribution of LATRA

For biodistribution studies, 50 μL of Cy5-co-loaded LATRA were intratumorally injected into MC38 tumor-bearing mice. At 4 or 24 h post-injection, the mice were euthanized, and tumors, tumor-draining lymph nodes (TDLNs), and major organs (heart, liver, spleen, lung, and kidney) were collected. The fluorescence distribution was then visualized using IVIS.

5.15. Anti-cancer studies

To investigate the therapeutic effects of LATRA in combination with RT, external beam X-ray irradiation (12 Gy) was administered to tumors on day 0. Six hours post-irradiation, 50 μL of LATRA solution (0.16 mg/mL) was intratumorally injected. The same dose of LATRA solution was subsequently injected into the tumors on days 3, 6,and 9. Tumor diameters were measured every three days, and tumor volumes were calculated using the formula: tumor volume = $(a \times b^2) / 2$, where "a" is the longest diameter and "b" is the shortest diameter of the tumor. Mice were euthanized when the tumor volume reached 1500 mm^3. To evaluate the effect of LATRA monotherapy, mice were intratumorally injected with 50 μL of LATRA solution (0.16 mg/mL) according to the same dosing schedule. To assess the dose-dependent anti-tumor efficacy of LATRA in combination with RT, mice received intratumoral injections of 50 μL of LATRA solution at either a low dose (0.08 mg/mL) or a high dose (0.16 mg/mL) following the same treatment regimen.

5.16. Immune memory studies

To assess the immune memory response induced by RT + LATRA treatment, cured MC38 tumor-bearing mice were re-challenged with MC38 tumor cells and monitored for tumor recurrence. On day 30 post-challenge, peripheral blood cells and spleen cells were isolated, followed by staining with anti-CD45-PerCP/Cy5.5, anti-CD3-APC, anti-CD4-PE/Cy7, anti-CD8-PE/Cy7, anti-CD44-FITC and anti-CD62L-PE for flow cytometry analysis.

5.17. Flow cytometry analyses of tumors, TDLNs, blood cells and spleens

MC38 tumors were irradiated with 12 Gy X-ray on day 0, followed by intratumorally injection of 50 μL of LATRA solution (0.16 mg/mL) on the same day and on days 3 and 6. On day 11 post-treatment, tumor tissues, tumor-draining lymph nodes (TDLNs), blood cells and spleens were collected for flow cytometry analysis.

5.17.1. Tumor tissues

Tumors were dissociated into single-cell suspensions, stained with Zombie NIR™ and incubated with anti-CD16/32 to block non-specific binding. After washing, the cells were stained with anti-CD45-PerCP/Cy5.5, anti-CD11b-FITC, anti-F4/80-PE, anti-CD86-PE/Cy7 and anti-CD206-APC for flow cytometry analysis.

5.17.2. TDLNs

TDLNs were dissociated into single-cell suspensions, stained with Zombie NIR™ and incubated with anti-CD16/32. After washing, the cells were stained with anti-CD45-PerCP/Cy5.5, anti-CD3-APC, anti-CD4-PE, anti-CD8-FITC and anti-CD69-PE/Cy7 for flow cytometry analysis.

5.17.3. Blood

Red blood cells were lysed using ACK lysis buffer. The remaining cells were stained with Zombie NIR™ and incubated with anti-CD16/32. After washing, the cells were stained with anti-CD45-PerCP/Cy5.5, anti-CD3-APC, anti-CD4-PE, anti-CD8-FITC and anti-CD69-PE/Cy7 for flow cytometry analysis.

5.17.4. Spleens

Spleens were dissociated into single-cell suspensions and red blood cells were lysed with ACK lysis buffer. The cells were stained with Zombie NIR™ and incubated with anti-CD16/32. After washing, the cells were divided into two groups for CD4 T cells staining and CD8 T cells staining, respectively. For CD4 T cells staining, the cells were stained with CD45-PerCP/Cy5.5, anti-CD3-APC, anti-CD4-PE/Cy7, anti-

CD44-FITC and anti-CD62L-PE for flow cytometry analysis. For CD8 T cells staining, the cells were stained with CD45-PerCP/Cy5.5, anti-CD3-APC, anti-CD8-PE/Cy7, anti-CD44-FITC and anti-CD62L-PE for flow cytometry analysis. For MDSCs staining, the cells were stained with CD45-PerCP/Cy5.5, anti-CD11b-FITC and anti-Gr-1-APC for flow cytometry analysis.

5.18. Inhibition of post-surgical breast tumor recurrence and metastasis

Ten days after inoculation with 4T1-Luc tumor cells, the tumors were surgically excised. After excision, gel/LATRA (8 μg of ATRA in 100 μL of gel) was applied to the surgical site. The next day, residual tumor tissue was irradiated with 12 Gy X-ray. Tumor recurrence and growth were monitored over time. At pre-determined time points, D-luciferin sodium salt (150 mg/kg) was intraperitoneally injected, and bioluminescent signals were analyzed using an IVIS imaging system 15 min post-injection. To assess tumor metastasis, lung tissues were collected on day 30 post-treatment for H&E staining to evaluate the formation of lung nodules.

5.19. Statistical analysis

All statistical analysis were performed using Prism 8 (GraphPad Software). For comparisons between two groups, an unpaired *t*-test was used. One-way ANOVA was used for comparisons between three or more groups. Survival curves were compared using a log-rank test. Data are presented as mean ± SD with a minimum of 3 biological replicates. For all graphs, $^{*}P < 0.05$; $^{**}P < 0.01$; $^{***}P < 0.001$.

Author contribution

H.H. and Y.Z. contributed equally to this work. H.H., Y.Z., Y.Z. and Z. Z. conceived the project. H.H., Y.Z., J.J. and C.Y. performed the experiments and analyzed the data. Y.Z., Y.S. and Y.P. provided technical input on this project. H.H., Y.Z. and Z.Z. drafted the manuscript. Y.Z. and Z.Z. supervised the project.

CRediT authorship contribution statement

Huilan He: Writing – original draft, Software, Methodology, Investigation, Formal analysis, Conceptualization. **Yun Zheng:** Software, Methodology, Investigation, Formal analysis, Conceptualization. **Jinlong Ji:** Software, Methodology, Investigation, Formal analysis. **Chunlian Ye:** Methodology, Investigation, Formal analysis. **Yu Sun:** Methodology, Investigation, Formal analysis. **Yuwei Peng:** Methodology, Investigation, Formal analysis. **Ying Zhang:** Writing – review & editing, Funding acquisition, Conceptualization. **Zhiyuan Zhong:** Writing – review & editing, Funding acquisition, Conceptualization.

Declaration of competing interest

The authors declare no conflict of interest.

Acknowledgments

This work was financially supported by the National Natural Science Foundation of China (52303199, 52233007), and the Natural Science Foundation of the Jiangsu Higher Education Institutions of China (23KJB350006).

Appendix A. Supplementary data

Supplementary data to this article can be found online at https://doi.org/10.1016/j.jconrel.2025.113995.

Data availability

The data that support the findings of this study are available from the corresponding author upon reasonable request.

References

[1] J.M. Price, A. Prabhakaran, C.M.L. West, Predicting tumour radiosensitivity to deliver precision radiotherapy, Nat. Rev. Clin. Oncol. 20 (2) (2023) 83–98.
[2] S. Demaria, E.B. Golden, S.C. Formenti, Role of local radiation therapy in cancer immunotherapy, JAMA Oncol. 1 (9) (2015) 1325–1332.
[3] L. Galluzzi, I. Vitale, S.A. Aaronson, et al., Molecular mechanisms of cell death: recommendations of the nomenclature committee on cell death 2018, Cell Death Differ. 25 (3) (2018) 486–541.
[4] L. Galluzzi, A. Buqué, O. Kepp, et al., Immunogenic cell death in cancer and infectious disease, Nat. Rev. Immunol. 17 (2) (2017) 97–111.
[5] L.L. Xu, C. Zou, S.S. Zhang, et al., Reshaping the systemic tumor immune environment (STIE) and tumor immune microenvironment (TIME) to enhance immunotherapy efficacy in solid tumors, J. Hematol. Oncol. 15 (1) (2022) 87.
[6] A. Filatenkov, J. Baker, A.M.S. Mueller, et al., Ablative tumor radiation can change the tumor immune cell microenvironment to induce durable complete remissions, Clin. Cancer Res. 21 (16) (2015) 3727–3739.
[7] S.C. Formenti, N.P. Rudqvist, E. Golden, et al., Radiotherapy induces responses of lung cancer to CTLA-4 blockade, Nat. Med. 24 (12) (2018) 1845–1851.
[8] W. Theelen, H.M.U. Peulen, F. Lalezari, et al., Effect of pembrolizumab after stereotactic body radiotherapy vs pembrolizumab alone on tumor response in patients with advanced non-small cell lung cancer: results of the PEMBRO-RT phase 2 randomized clinical trial, JAMA Oncol. 5 (9) (2019) 1276–1282.
[9] R.B. Patel, M. Ye, P.M. Carlson, et al., Development of an in situ cancer vaccine via combinational radiation and bacterial-membrane-coated nanoparticles, Adv. Mater. 31 (43) (2019) e1902626.
[10] Y. Wu, Y.Q. Song, R.Z. Wang, et al., Molecular mechanisms of tumor resistance to radiotherapy, Mol. Cancer 22 (1) (2023) 96.
[11] C.A.M. La Porta, S. Zapperi, Complexity in cancer stem cells and tumor evolution: toward precision medicine, Semin. Cancer Biol. 44 (2017) 3–9.
[12] J. Agudo, Y.X. Miao, Stemness in solid malignancies: coping with immune attack, Nat. Rev. Cancer 25 (1) (2025) 27–40.
[13] A. Grover, E. Sanseviero, E. Timosenko, et al., Myeloid-derived suppressor cells: a propitious road to clinic, Cancer Discov. 11 (11) (2021) 2693–2706.
[14] H. de Thé, Differentiation therapy revisited, Nat. Rev. Cancer 18 (2) (2018) 117–127.
[15] M.A. Caricasulo, A. Zanetti, M. Terao, et al., Cellular and micro-environmental responses influencing the antitumor activity of all-trans retinoic acid in breast cancer, Cell Commun. Signal 22 (1) (2024) 127.
[16] S. Shen, X. Xu, S. Lin, et al., A nanotherapeutic strategy to overcome chemotherapeutic resistance of cancer stem-like cells, Nat. Nanotechnol. 16 (1) (2021) 104–113.
[17] R. Ferreira, J. Napoli, T. Enver, et al., Advances and challenges in retinoid delivery systems in regenerative and therapeutic medicine, Nat. Commun. 11 (1) (2020) 4265.
[18] E. Jung, N. Song, Y. Lee, et al., H2O2-activatable hybrid prodrug nanoassemblies as a pure nanodrug for hepatic ischemia/reperfusion injury, Biomaterials 284 (2022) 121515.
[19] S.Y. Lee, E.K. Jeong, M.K. Ju, et al., Induction of metastasis, cancer stem cell phenotype, and oncogenic metabolism in cancer cells by ionizing radiation, Mol. Cancer 16 (2017) 10.
[20] J.M. Hsu, W.Y. Xia, Y.H. Hsu, et al., STT3-dependent PD-L1 accumulation on cancer stem cells promotes immune evasion, Nat. Commun. 9 (2018) 1908.
[21] N. Erin, J. Grahovac, A. Brozovic, et al., Tumor microenvironment and epithelial mesenchymal transition as targets to overcome tumor multidrug resistance, Drug Resist. Updat. 53 (2020) 100715.
[22] Y. Sun, L. Liu, H. He, et al., Co-activating STING-TLR9 pathways promotes radiotherapy-induced cancer vaccination, J. Control. Release 379 (2025) 327–343.
[23] S. Gkountela, F. Castro-Giner, B.M. Szczerba, et al., Circulating tumor cell clustering shapes DNA methylation to enable metastasis seeding, Cell 176 (1–2) (2019) 98.
[24] Z. Li, J. Yang, B. Ren, et al., Double-layered hollow mesoporous cuprous oxide nanoparticles for double drug sequential therapy of tumors, Adv. Mater. 36 (2024) 2313212.
[25] C. Peitzsch, A. Tyutyunnykova, K. Pantel, et al., Cancer stem cells: the root of tumor recurrence and metastases, Semin. Cancer Biol. 44 (2017) 10–24.
[26] A.Q. Shang, C.Z. Gu, W.W. Wang, et al., Exosomal circPACRGL promotes progression of colorectal cancer via the miR-142-3p/miR-506-3p-TGF-β1 axis, Mol. Cancer 19 (1) (2020) 117.
[27] Y.Y. Wang, Y. Xiang, W.X. Xin, et al., Dendritic cell biology and its role in tumor immunotherapy, J. Hematol. Oncol. 13 (1) (2020) 107.
[28] S. Chen, A.F.U.H. Saeed, Q. Liu, et al., Macrophages in immunoregulation and therapeutics, Signal Transduct. Target. Ther. 8 (1) (2023) 207.
[29] Y. Zheng, Y. Han, T. Wang, et al., Reprogramming tumor-associated macrophages via ROS-mediated novel mechanism of ultra-small Cu2−xSe nanoparticles to enhance anti-tumor immunity, Adv. Funct. Mater. 32 (12) (2021) 2108971.
[30] Y. Kim, S. Lee, S. Jon, Liposomal delivery of an immunostimulatory CpG induces robust antitumor immunity and long-term immune memory by reprogramming tumor-associated macrophages, Adv. Healthc. Mater. 13 (6) (2023) 2300549.

[31] Q. Chen, C. Wang, X. Zhang, et al., In situ sprayed bioresponsive immunotherapeutic gel for post-surgical cancer treatment, Nat. Nanotechnol. 14 (1) (2019) 89–97.
[32] J. Xu, J. Lv, Q. Zhuang, et al., A general strategy towards personalized nanovaccines based on fluoropolymers for post-surgical cancer immunotherapy, Nat. Nanotechnol. 15 (12) (2020) 1043–1052.
[33] X. Guan, L. Sun, Y. Shen, et al., Nanoparticle-enhanced radiotherapy synergizes with PD-L1 blockade to limit post-surgical cancer recurrence and metastasis, Nat. Commun. 13 (1) (2022) 2834.
[34] R.P. Tobin, D.T. Cogswell, V.M. Cates, et al., Targeting MDSC differentiation using ATRA: a phase I/II clinical trial combining pembrolizumab and all-trans retinoic acid for metastatic melanoma, Clin. Cancer Res. 29 (7) (2023) 1209–1219.
[35] Y. Zhu, T. Liu, X. Deng, et al., Ultrasound-mediated intra−/extracellular dual intervening effect combined with all-trans retinoic acid for cancer stemness inhibition, Nano Today 55 (2024) 102207.
[36] B. Wang, J. Zhou, R. Li, et al., Activating CD8(+) T cells by Pt(IV) prodrug-based nanomedicine and aPD-L1 antibody for enhanced cancer immunotherapy, Adv. Mater. 36 (2024) e2311640.